the slabs' sinking velocities in the lower mantle, not from sluggish relaxation of the rotational bulge in response to changes in inertia. The bulge effect is present in our calculations, but the changes in **C** due to subduction were so slow during the last 60 million years that the relaxation of the bulge was not the limiting factor; it is mainly the slow variation in **C** that controls the rates of polar wander. All three models yield similar amounts of long-term polar wander, especially over the past 60 million years, when rates were always less than 1° per million years. For the $VR = 30$ model, the rates were <0.5° per million years since the beginning of the Tertiary, with only about 10° total latitudinal drift of the rotation axis since 50 Ma, or an average of about 0.2° per million years, a rate that falls within the observational constraints on TPW (Fig. 1A). The $VR = 30$ model also gives a good fit to the present-day geoid (*15*).

Comparison (Fig. 1B) of the polar wander paths predicted by isoviscous ($VR = 1$) and layered viscosity ($VR = 30$) models in the same reference frame (*26*) as that for the observed paths (Fig. 1A) shows a strong sensitivity of the TPW path to variations in viscosity structure. Although the details of the various observed curves also vary greatly, the $VR = 30$ model does yield a reasonable overall amplitude for TPW since 100 Ma, and the predicted TPW since the early Tertiary (50 to 60 Ma) is about 5° to 10° toward Greenland, roughly in accord with observation. The latter result is also consistent with Jurdy's (*27*) empirical analysis of polar wander resulting from changes in Cenozoic subduction. The model paths for before Tertiary time are not very meaningful because subduction history becomes less well constrained in the time frame of 100 to 200 Ma. Nevertheless, the low observed rate of TPW is explained by relatively slow changes in the global pattern of subduction zones.

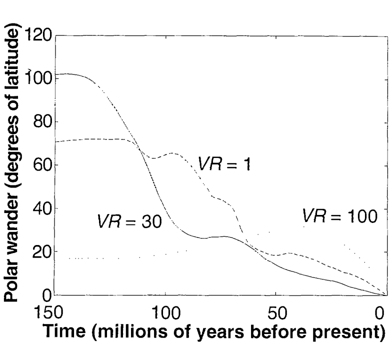

Fig. 3. Distance in degrees (latitude) between the position of the rotation axis at time zero (present) and the position at times in the past for the three different mantle viscosity models. These curves are computed from solutions to the full, nonlinear Euler equations 1 given in (*13*).

REFERENCES AND NOTES

1. R. G. Gordon, *Annu. Rev. Earth Planet. Sci.* **15**, 567 (1987).
2. W. J. Morgan, in *The Sea*, C. Emiliani, Ed. (Wiley, New York, 1981), vol. 7, pp. 443–487.
3. D. M. Jurdy, *Tectonophysics* **74**, 1 (1981).
4. R. A. Livermore, F. J. Vine, A. G. Smith, *Geophys. J. R. Astron. Soc.* **79**, 939 (1984).
5. J. Andrews, *J. Geophys. Res.* **90**, 7737 (1985).
6. J. Besse and V. Courtillot, *ibid.* **96**, 4029 (1991).
7. This long-term TPW is in the same direction as, although much smaller in amplitude than, the present-day polar wander, which is attributed to postglacial rebound. See, for example, S. R. Dickman, *Geophys. J. R. Astron. Soc.* **51**, 229 (1977); (*19*).
8. T. Gold, *Nature* **175**, 526 (1955).
9. P. Goldreich and A. Toomre, *J. Geophys. Res.* **74**, 2555 (1969).
10. P. J. Tackley, thesis, California Institute of Technology (1994); M. A. Richards, Y. Ricard, H.-P. Bunge, *Eos* **75**, 67 (1994); in preparation.
11. C. G. Chase, *Annu. Rev. Earth Planet. Sci.* **13**, 97 (1985).
12. G. Spada, Y. Ricard, R. Sabadini, *Nature* **360**, 452 (1992).
13. Y. Ricard, G. Spada, R. Sabadini, *Geophys. J. Int.* **113**, 284 (1993).
14. R. Sabadini, D. A. Yuen, E. Boschi, *J. Geophys. Res.* **89**, 7609 (1984); R. Sabadini and D. A. Yuen, *Nature* **339**, 373 (1989).
15. Y. Ricard, M. A. Richards, C. Lithgow-Bertelloni, Y. LeStunff, *J. Geophys. Res.* **98**, 21895 (1993).
16. W. Munk and G. J. F. MacDonald, *The Rotation of the Earth: A Geophysical Discussion* (Cambridge Univ. Press, London, 1960).
17. M. A. Richards and B. H. Hager, *J. Geophys. Res.* **89**, 5987 (1984); Y. Ricard, L. Fleitout, C. Froidevaux, *Ann. Geophys.* **2**, 267 (1984).
18. G. Spada, thesis, University of Bologna (1992).
19. R. Sabadini and W. R. Peltier, *Geophys. J. R. Astron. Soc.* **66**, 553 (1981).
20. M. A. Richards and D. C. Engebretson, *Nature* **355**, 437 (1992).
21. D. C. Engebretson, K. P. Kelly, H. J. Cashman, M. A. Richards, *GSA Today* **2**, 93 (1992).
22. C. Lithgow-Bertelloni and M. A. Richards, *Rev. Geophys.*, in press.
23. ______, *Geophys. Res. Lett.* **22**, 1317 (1995).
24. B. H. Hager and M. A. Richards, *Philos. Trans. R. Soc. London Ser. A* **328**, 309 (1989); S. D. King and T. G. Masters, *Geophys. Res. Lett.* **19**, 1551 (1992); J. X. Mitrovica, *J. Geophys. Res.* **101**, 555 (1996).
25. M. Gurnis, thesis, Australian National Univ. (1986); M. A. Richards, in *Glacial Isostasy, Sea Level and Mantle Rheology*, R. Sabadini *et al.*, Eds. (Kluwer Academic, Hingham, MA, 1991), pp. 571–588.
26. The polar wander paths in Fig. 1B are calculated somewhat differently than the simpler latitudinal variation curves in Fig. 3. In Fig. 1B, we have compensated for the fact that the subduction heterogeneity model does not yield the correct present-day degree 2 geoid (for example, the C_{21} and S_{21} harmonic coefficients are nonzero). This mismatch results from model error of an undetermined nature (*15*). The compensation is achieved by subtracting the mismatched off-diagonal terms in the present-day inertia tensor from the calculations at all times, so that the present-day model rotation pole position corresponds exactly to Earth's North Pole; otherwise, the model and observed curves would not be comparable in any meaningful way because the model curves would begin at some latitude different from the North Pole. This solution is not entirely satisfactory, but it provides a way to compare the overall amplitudes of the TPW curves. Comparison between the detailed shapes of the observed and model TPW paths are probably not very meaningful because of the uncertainties in observations and the necessary compensation of the model curves.
27. D. M. Jurdy, *J. Geophys. Res.* **88**, 6395 (1983).

28. M.A.R. was supported by NSF grants EAR-9117538 and EAR-9629376 and is grateful to C. Froidevaux of the Ecole Normale Superieure, Paris, for support as a visiting scholar. R. Gordon and D. Jurdy provided helpful reviews of the original manuscript.

12 August 1996; accepted 22 November 1996

Depletion of the Outer Asteroid Belt

Jer-Chyi Liou* and Renu Malhotra

During the early history of the solar system, it is likely that the outer planets changed their distance from the sun, and hence, their influence on the asteroid belt evolved with time. The gravitational influence of Jupiter and Saturn on the orbital evolution of asteroids in the outer asteroid belt was calculated. The results show that the sweeping of mean motion resonances associated with planetary migration efficiently destabilizes orbits in the outer asteroid belt on a time scale of 10 million years. This mechanism provides an explanation for the observed depletion of asteroids in that region.

Asteroids are small, rocky bodies less than 1000 km in diameter that lie between the orbits of Mars and Jupiter in the region traditionally called the asteroid belt. The outer asteroid belt, from 3 to 5 astronomical units (AU) from the sun, is nonuniform and depleted of asteroids. The orbital eccentricities and inclinations, as functions of semimajor axes, of 7100 numbered asteroids (*1*) (Fig. 1) show four major features: (i) a lack of asteroids in the 1 : 2 interior mean motion resonance (MMR) (*2*) with Jupiter centered at 3.28 AU, (ii) a lack of asteroids between 3.5 and 3.9 AU, (iii) a concentration of asteroids in the 2 : 3 interior MMR with Jupiter centered at 3.97 AU, and (iv) a lack of asteroids beyond the 2 : 3 interior MMR.

The "gravitational hypothesis" (*3*) postulates that the gravitational forces of the planets are responsible for shaping the asteroid belt. This hypothesis has explained

J.-C. Liou, SN3, NASA Johnson Space Center, Houston, TX 77058, USA.
R. Malhotra, Lunar and Planetary Institute, Houston, TX 77058, USA.

*To whom correspondence should be addressed. E-mail: liou@sn3.jsc.nasa.gov

gaps at the 1:3 and 1:2 interior MMR locations and the depletion beyond the 2:3 interior MMR (*4–6*). However, recent numerical simulations of the solar system for a period of 1 billion years based on this hypothesis have failed to reproduce the observed lack of asteroids between 3.5 and 3.9 AU, prompting the conjecture that this feature may be related to the distribution of asteroids at the end of planetary formation or to other nongravitational processes (*7, 8*). Here we consider the planet migration hypothesis that has been invoked for several outer solar system problems (*9, 10*).

During the early history of the solar system, it is likely that gravitational scattering of planetesimals by giant planets caused the orbits of Saturn, Uranus, and Neptune to migrate outward and the orbit of Jupiter to migrate inward (*11*). This dynamical process, if it occurred, would explain the peculiar orbit of Pluto and the capture of Kuiper Belt objects in MMRs with Neptune (*9, 10*). The migration of the giant planets would also have affected the evolution of the main belt asteroids and may have been responsible for some of the hitherto unsolved mysteries of the observed structure of the asteroid belt (*9*). We numerically calculated the orbital evolution of 200 test asteroids initially in near-circular, low-inclination orbits in the outer asteroid belt under the perturbing forces of Jupiter and Saturn—when the planets are in their current orbits and when they are in radial migration—to determine how planetary migration would have affected the asteroid distribution.

We used two numerical integration methods: an implicit Runge-Kutta integrator with a self-adjusting step-size control (RADAU) (*12*) and a modified mixed-variable quasi-symplectic mapping (*13*). RADAU handles close encounters between a test asteroid and a planet accurately, but its slow calculation speed makes it impractical for a systematic study of the evolution of a large number of asteroids over 10 million years. The mapping method is at least one order of magnitude faster than RADAU, so it is suitable for studying the long-term evolution of test asteroids; however, it is not accurate for close encounters, so we terminated the integration of any asteroid that had a close encounter with any planet (*14*) and presumed that it had been removed from the asteroid population. We compared the results of simulations using both integrators for integration times less than 10 million years and found that, statistically, both integrators gave the same results. For integrations longer than 10 million years, we used only the mapping integrator.

We modeled the migration of a planet by applying a force opposite to (or along) its orbital velocity vector such that it migrated radially inward (or outward) over time. We included two planets in our simulations: Jupiter with a 0.2-AU inward migration and Saturn with a 0.8-AU outward migration. We used two migration schemes: (i) a linear migration, wherein the planetary semimajor axes changed linearly with time, and (ii) an exponential migration, wherein the rates of change of planetary semimajor axes decayed exponentially with time, with migration time scales ranging from 1 million to 10 million years. The total integration times ranged from 1 million to 100 million years. Hundreds of test asteroids were initially placed between 3.2 and 4.2 AU. Their initial orbital eccentricities and inclinations were randomly chosen between 0 and 0.1 and between 0° and 6°, respectively. Their initial longitudes of ascending node, longitudes of pericenter, and mean longitudes were all randomly chosen between 0° and 360°. Once the initial conditions of test asteroids and planets were set up, their equations of motion were numerically integrated. In our calculations, the planets fully interacted with each other and acted on test asteroids, whereas the test asteroids did not affect the motions of planets.

Our simulation with no planet migration (Fig. 2B) is consistent with previous work: (i) most asteroids at the 1:2 interior MMR were depleted (*5*), (ii) asteroids at the 2:3 interior MMR were maintained in stable resonance, (iii) asteroids outside 4 AU were removed by close encounters with Jupiter (*6*), and (iv) the depletion of asteroids between 3.5 and 3.9 AU was only about 50% (*7*). The latter depletion fraction did not increase even with a 10-fold longer integration of 1 billion years (*8*). On the other hand, in our simulations with planetary migration, the orbital migration of giant planets produced an efficient depletion in the region between 3.5 and 3.9 AU on million-year time scales (Fig. 2, C through E). The linear and exponential migration simulations gave similar results. They also indicate that the slower the planets migrate, the more efficient the depletion is.

Planet migration increased the efficiency of depletion of asteroids in this particular region because the depletion was caused by the sweeping of MMRs through the region as Jupiter migrated inward. It has been shown recently that, in the current planetary configuration, asteroids at the 4:7, 3:5, and 5:8 interior MMRs with Jupiter (located at 3.58, 3.70, and 3.80 AU, respectively) are unstable over million-year time scales (*8, 15*). The orbit of an asteroid in one of those three resonances is highly chaotic: An initially circular orbit at these resonances will have its orbital eccentricity pumped up in a short period of time; eventually its orbit crosses that of Jupiter, and close encounters with the planet remove it from that region. It is these three MMRs that provide the 50% depletion of asteroids from the outer

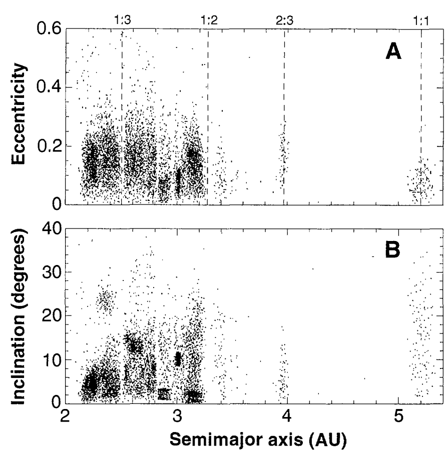

Fig. 1. Distribution of the observed asteroids between 2 and 5.4 AU on the basis of their orbital eccentricities (**A**) and inclinations (**B**) as functions of semimajor axes. The gaps and concentrations of asteroids are associated with the mean motion resonances with Jupiter. The locations of four of them—1:3, 1:2, 2:3, and 1:1—are shown by dashed lines in (A).

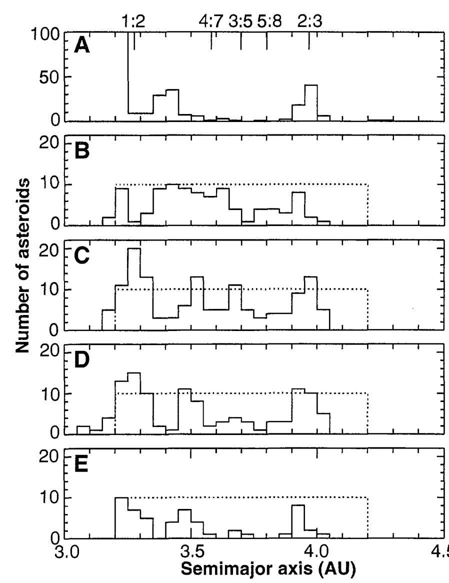

Fig. 2. (**A**) Distribution of the observed numbered asteroids. The locations of the 1:2, 4:7, 3:5, 5:8, and 2:3 interior MMRs are labeled by the bold line segments at the top. (**B**) Distribution of 200 test asteroids after 100 million years of numerical simulation in a sun-Jupiter-Saturn-asteroids system [adapted from (*16*)]. Jupiter and Saturn are interacting with each other with no radial migration. The dotted line indicates the initial distribution of the test asteroids. The 1:2 gap was formed after 10 million years. About 50% of the original asteroids still remained between 3.5 and 3.9 AU at the end of the simulation. (**C**), (**D**), and (**E**) show results from three different numerical simulations of sun-Jupiter-Saturn-asteroids systems in which Jupiter migrated inward while Saturn migrated outward linearly with time for 1, 2, and 8 million years, respectively. Simulations with exponential migration gave similar results.

belt in the classical case (no planet migration). When the migration of giant planets is included or, more specifically, when the inward migration of Jupiter is included, those three resonances sweep through the region between 3.5 and 3.9 AU. Asteroids originally not in any resonances encounter those MMRs and get captured, and their orbits become chaotic (Fig. 3). It is this resonance-sweeping mechanism that depletes asteroids from the outer belt.

We also considered the effect of this mechanism on other parts of the asteroid belt. Asteroids outside 4 AU were removed, whereas asteroids were maintained in the 2:3 interior MMR at 3.97 AU (Fig. 2), consistent with the observed asteroid distribution. However, in our simulations, asteroids were captured and maintained in the 1:2 interior MMR at 3.28 AU, contrary to the observed gap at this location. A plausible explanation for this deficiency is the time scale of instability for asteroids in that resonance. In the classical case (no planet migration), the time scale to clear the 1:2 gap is on the order of 10 million years (*5*, *16*). A hint of this long-term effect is evident in Fig. 2E and is more obvious in Fig. 2B. We conclude that the asteroids at the 1:2 interior MMR were removed by the long-term perturbations of the planets after planet migration ceased (*17*).

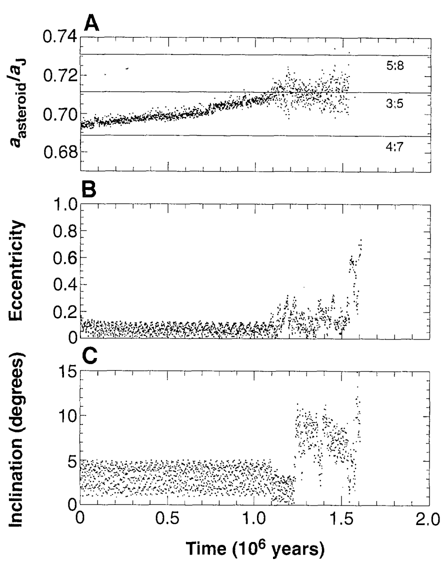

Fig. 3. Evolution of an asteroid in a sun-Jupiter-Saturn-asteroid system. The planetary migration time is 2 million years. (**A**) Semimajor axis of the test asteroid normalized to the semimajor axis of Jupiter. Three horizontal lines show the locations of the 5:8, 3:5, and 4:7 interior MMRs. As Jupiter migrated inward, the relative semimajor axis of the asteroid increased. This test asteroid was initially not in any MMR with Jupiter; however, the inward motion of Jupiter caused the 3:5 interior MMR to sweep by and capture this asteroid into resonance at 1.1 million years. The eccentricity (**B**) and inclination (**C**) of the asteroid varied irregularly when it was in resonance. Finally, its eccentricity increased to such an extent that it began to cross the orbit of Jupiter, and subsequent close encounters with the giant planet finally made its orbit hyperbolic and removed it from the outer belt.

REFERENCES AND NOTES

1. E. Bowell, *Asteroid Orbital Elements Database* (Lowell Observatory, Flagstaff, AZ, 1996).
2. S. F. Dermott and C. D. Murray, *Nature* **301**, 201 (1983). A MMR occurs when the orbital period of an asteroid is a simple multiple of Jupiter's orbital period. In addition to 1:2 and 2:3, interior MMRs are also associated with other gaps in the asteroid belt.
3. R. Greenberg and H. Scholl, in *Asteroids*, T. Gehrels, Ed. (Univ. of Arizona Press, Tucson, 1979), pp. 310–333; A. M. Nobili, in *Asteroids II*, R. P. Binzel, T. Gehrels, M. S. Matthews, Eds. (Univ. of Arizona Press, Tucson, 1989), pp. 862–879.
4. J. Wisdom, *Icarus* **72**, 241 (1987).
5. F. A. Franklin, *Astron. J.* **112**, 1247 (1996); A. Morbidelli, *ibid.* **111**, 2453 (1996).
6. B. Gladman and M. Duncan, *ibid.* **100**, 1680 (1990).
7. M. Lecar, F. Franklin, P. Soper, *Icarus* **96**, 234 (1992).
8. M. Duncan, in *Circumstellar Dust Disks and Planet Formation*, R. Ferlet and A. Vidal-Madjar, Eds. (Editions Frontieres, Gif-sur-Yvette, 1994), pp. 245–255.
9. R. Malhotra, *Nature* **365**, 819 (1993).
10. ———, *Astron. J.* **110**, 420 (1995).
11. J. A. Fernández and W.-H. Ip, *Icarus* **58**, 109 (1984); *Planet. Space Sci.* **44**, 431 (1996).
12. E. Everhart, in *Dynamics of Comets: Their Origin and Evolution*, A. Carusi and G. B. Valsecchi, Eds. (Reidel, Boston, 1985), pp. 185–202.
13. R. Malhotra, *Celestial Mech. Dyn. Astron.* **60**, 373 (1994).
14. Integration of a test asteroid was stopped, and the asteroid was presumed to have been removed from the population, if it came within 1 Hill radius r_H of a planet. Once an object is less than 1 r_H from a planet, the dominant perturber is the planet, not the sun. The Hill radii of Jupiter and Saturn are 0.36 and 0.44 AU, respectively.
15. M. J. Holman and N. W. Murray, *Astron. J.* **112**, 1278 (1996).
16. R. Malhotra, unpublished material.
17. Because of the geometric locations of the 4:7, 3:5, and 5:8 interior MMRs, Jupiter has to migrate inward, by about 0.2 AU, to remove asteroids in the 3.5- to 3.9-AU region. However, the migration time scale and the migration scheme (linear, exponential, or other) are less constrained on the basis of the population of asteroids in this region. The long-term dynamics of the asteroids at 2:3 and 1:2 interior MMRs after the planet migration ceased may provide more insight into these questions.

18. We thank H. Zook for enthusiastic discussions. This research was performed while J.-C.L. held a National Research Council–NASA Johnson Space Center Research Associateship and R.M. was a staff scientist at the Lunar and Planetary Institute (LPI), which is operated by the Universities Space Research Association under contract NASW-4574 with NASA. Support was also provided by NASA's Origins of Solar Systems Research Program under grant 4474. This paper is LPI contribution 905.

4 September 1996; accepted 15 November 1996

Kinetic Measurement of the Step Size of DNA Unwinding by *Escherichia coli* UvrD Helicase

Janid A. Ali and Timothy M. Lohman*

The kinetic mechanism by which the DNA repair helicase UvrD of *Escherichia coli* unwinds duplex DNA was examined with the use of a series of oligodeoxynucleotides with duplex regions ranging from 10 to 40 base pairs. Single-turnover unwinding experiments showed distinct lag phases that increased with duplex length because partially unwound DNA intermediate states are highly populated during unwinding. Analysis of these kinetics indicates that UvrD unwinds duplex DNA in discrete steps, with an average "step size" of 4 to 5 base pairs (approximately one-half turn of the DNA helix). This suggests an unwinding mechanism in which alternating subunits of the dimeric helicase interact directly with duplex DNA.

DNA helicases are motor proteins that function to unwind duplex (ds) DNA during DNA replication, recombination, and repair and are also components of eukaryotic transcription complexes (*1*, *2*). These enzymes use the chemical energy obtained from nucleoside triphosphate binding or hydrolysis (or both) to perform the mechanical work of unwinding dsDNA, which also requires translocation of the helicase along DNA for processive unwinding.

The *Escherichia coli* UvrD helicase [helicase II (*3*)] plays essential roles in both methyl-directed mismatch repair (*4*) and nucleotide excision repair of DNA (*5*), and in humans, defects in these processes are linked to increased susceptibility to cancer (*6*). UvrD protein [720 amino acids; molecular mass of 81,989 (*7*)] forms dimers in the absence of DNA (*8*), and the dimeric form of the enzyme is functional in DNA unwinding (*9*). In fact, the functional forms of most DNA helicases are oligomeric (mainly dimers or hexamers), most likely because multiple DNA binding sites are needed for helicase function (*1*, *10*, *11*). UvrD displays a 3′-to-5′ polarity in DNA unwinding (*12*), in that a 3′ single-stranded (ss) DNA flanking the duplex facilitates initiation of unwinding in vitro (*9*); however, UvrD can also initiate unwinding at a nick (*13*). UvrD shares about

Department of Biochemistry and Molecular Biophysics, Washington University School of Medicine, 660 South Euclid Avenue, Box 8231, St. Louis, MO 63110, USA.

*To whom correspondence should be addressed.